Biochimica et Biophysica Acta 1853 (2015) 522–534

Contents lists available at ScienceDirect

Biochimica et Biophysica Acta

journal homepage: www.elsevier.com/locate/bbamcr

Depletion of poly(A)-specific ribonuclease (PARN) inhibits proliferation of human gastric cancer cells by blocking cell cycle progression

Li-Na Zhang, Yong-Bin Yan *

State Key Laboratory of Biomembrane and Membrane Biotechnology, School of Life Sciences, Tsinghua University, Beijing 100084, China

ARTICLE INFO

Article history:
Received 31 July 2014
Received in revised form 2 December 2014
Accepted 3 December 2014
Available online 11 December 2014

Keywords:
Poly(A)-specific ribonuclease
Cell cycle arrest
p21
p53
mRNA stability
Tumor heterogeneity

ABSTRACT

Regulation of mRNA decay plays a crucial role in the post-transcriptional control of cell growth, survival, differentiation, death and senescence. Deadenylation is a rate-limiting step in the silence and degradation of the bulk of highly regulated mRNAs. However, the physiological functions of various deadenylases have not been fully deciphered. In this research, we found that poly(A)-specific ribonuclease (PARN) was upregulated in gastric tumor tissues and gastric cancer cell lines MKN28 and AGS. The cellular function of PARN was investigated by stably knocking down the endogenous PARN in the MKN28 and AGS cells. Our results showed that PARN-depletion significantly inhibited the proliferation of the two types of gastric cancer cells and promoted cell death, but did not significantly affect cell motility and invasion. The depletion of PARN arrested the gastric cancer cells at the G_0/G_1 phase by upregulating the expression levels of p53 and p21 but not p27. The mRNA stability of *p53* was unaffected by PARN-knockdown in both types of cells. A significant stabilizing effect of PARN-depletion on *p21* mRNA was observed in the AGS cells but not in the MKN28 cells. We further showed that the *p21* 3′-UTR triggered the action of PARN in the AGS cells. The dissimilar observations between the MKN28 and AGS cells as well as various stress conditions suggested that the action of PARN strongly relied on protein expression profiles of the cells, which led to heterogeneity in the stability of PARN-targeted mRNAs.

1. Introduction

Regulation of gene expression is crucial for almost all physiological and pathological processes. The number of active transcripts in the cytoplasm is determined by a number of rate-limiting steps including transcription, processing, transportation, localization, translation repression and decay [1,2]. The fate of a mature mRNA is predominantly regulated by the untranslational region (UTR) at the 5′- and 3′-end. Particularly, the bulk of eukaryotic mRNAs contain a long template-independent poly(A) tail at the 3′-end. The shortening of the poly(A) tail, which is called deadenylation, is the rate-limiting step of the degradation of most eukaryotic mRNAs [3]. Deadenylation is executed by deadenylases, which are a group of 3′-exoribonucleases with a high preference of poly(A) as the substrate. In most organisms, there are a number of deadenylases with distinct domain compositions and physiological functions [2,4]. According to the nature of the nuclease domain, deadenylases are divided into two classes: the endonuclease–exonuclease–phosphatase (EEP) superfamily and the DEDD/DnaQ-like 3′–5′ exonuclease domain superfamily. The EEP superfamily contains various Ccr4 orthologs and PDE12, while the Caf1 orthologs and poly(A)-specific ribonuclease (PARN) belong to the DEDD superfamily. The various deadenylases and their binding partners are evolved to endow the cell diverse methods to regulate mRNA turnover [2,4].

By modulating the poly(A) tail length of mRNAs and mRNA fates thereby, deadenylases have been found to participate in many vital cellular processes such as mitotic division, oocyte maturation, differentiation and responses to various stresses [2,4–8]. Whenever there is a need of metabolic changes, the fates of a certain subset of mRNAs will be regulated by either enhancing or decreasing mRNA stability. For instance, the cells undergo dramatic changes to cease both transcription and translation during mitosis. Thus the cell cycle progression is not only regulated by the accumulation and modification of executed proteins but also the number of active transcripts [9]. Basically, the cell cycle is controlled by cyclin-dependent kinases (CDKs) and the associated activators and inhibitors [10]. The Cip/Kip family proteins, which include $p21^{Waf1/Cip1}$ (p21), $p27^{kip1}$ (p27) and $p57^{kip2}$ (p57) are well-characterized CDK inhibitors in regulating cell cycle phase transitions from G_1 to S and G_2 to M [10,11]. Among them, p21, an important transcriptional target of p53 [12], is a critical regulator of many physiological

Abbreviations: BSA, bovine serum albumin; CDK, cyclin-dependent kinase; DDR, DNA damage response; DMEM, Dulbecco's modified Eagle's medium; EEP, endonuclease–exonuclease–phosphatase; HRP, Horseradish peroxidase; HU, hydroxyl urea; M-MLV, Moloney murine leukemia virus; MTS, 3-(4,5-dimethylthiazol-2-yl)-5-(3-carboxymethoxyphenyl)-2-(4-sulfophenyl)-2H-tetrazolium, inner salt; P-body, processing body; PARN, poly(A)-specific ribonuclease; PARP, poly(ADP-ribose) polymerase; PBS, phosphate-buffered saline; PI, propidium iodide; SDS, sodium dodecyl sulfate; UTR, untranslational region of mRNA

* Corresponding author at: School of Life Sciences, Tsinghua University, Beijing 100084, China. Tel.: +86 10 6278 3477; fax: +86 10 6277 2245.
E-mail address: ybyan@tsinghua.edu.cn (Y.-B. Yan).

http://dx.doi.org/10.1016/j.bbamcr.2014.12.004
0167-4889/

and pathological processes involving development, stem cell renewal, senescence and tumorigenesis [13,14].

In addition to transcriptional regulation by p53, the protein level of p21 is also controlled by regulators affecting *p21* mRNA stability or p21 protein stability [14,15]. Similar to the other highly regulated mRNAs, the *p21* mRNA possesses a long 3′-UTR of ~1500 nt, which contains binding sites of various miRNAs and RNA-binding proteins [15]. One of the most characterized *cis*-acting elements at the 3′-UTR of *p21* is the AU-rich element (ARE), which recruits several ARE-binding proteins such as the Hu/Elav family proteins. miRNAs are generally destabilizing, while the RNA-binding proteins can either enhance or reduce mRNA stability. Previous studies have shown that the *p21* mRNA can be stabilized by the Hu/Elav family proteins [16,17], RBM24 [18], RNPC1/RBM38 [19], ZONAB/DbpA [20] and Ccr4d/ANGEL2 [21], while be destabilized by the KH-domain containing proteins [22,23] and FXR1P [24]. It seems that the increase of *p21* mRNA stability is associated with the p53 signaling pathway since most of the above stabilizing factors are targets of p53, while the reduction of *p21* mRNA stability is usually p53-independent.

Considering that most regulated mRNAs are degraded via the deadenylation-dependent pathway [25], deadenylases are expected to participate in the regulation of *p21* mRNA stability. However, only Ccr4d/ANGEL2 has been characterized thus far to elevate *p21* mRNA stability by binding with the 3′-UTR directly [21]. Meanwhile, the depletion of Ccr4b/CNOT6L in NIH 3T3 cells increases the mRNA stability of *p27* but not *p21* [26]. Among the various deadenylases, PARN is unique due to its highly processive deadenylation activity in a cap-dependent manner (reviewed in [5]). PARN has been shown to participate in rapid deadenylation mediated by ARE [27], which has been shown to be a stabilizing element in the *p21* mRNA. PARN can be recruited to the ARE-containing mRNAs by the KH-domain containing proteins [28], tristetraprolin (TTP) [29], CUG-BP [30] and exosome [27]. Since two of the Ccr4 family proteins have been shown to have no impacts on the promotion of *p21* mRNA deadenylation [21,26], herein we asked whether PARN plays such a role in the cells. The proposal of *p21* mRNA deadenylation triggered by PARN can be indirectly supported by several physiological functions of PARN. Recently it has been shown that PARN is involved in DNA-damage response via the p38MAPK/MK2 pathway [31] and/or recruitment by CstF-50 [32]. Knockdown of PARN increases the migration rate of mouse myoblasts [33]. Moreover, PARN has been found to have a high expression level in acute leukemias [34]. These observations suggest that PARN plays a role in cellular processes involving the action of p21. To further elucidate the cellular functions of PARN, the expression of PARN was stably knocked down in two human gastric cancer cell lines, MKN28 and AGS. Our results showed that depletion of PARN resulted in cell proliferation inhibition and cell cycle arrest at the G_0/G_1 phase. Furthermore, we showed that depletion of PARN led to a significant increase of p21 expression. However, the two gastric cancer cell lines showed heterogeneity in response to PARN knockdown. The increased p21 expression in MKN28 cells was more likely to be caused by the compensatory upregulation of the other deadenylases such as Ccr4d, while that in AGS cells was due to the stabilization of the *p21* mRNA induced by PARN-depletion directly.

2. Materials and methods

2.1. Materials

Rabbit anti-PARN and anti-Dcp1a antibodies were from Abcam. Antibodies against human Ccr4a, cyclin D1, cyclin E2, CDK2, CDK4, p21, p27, p53, poly(ADP-ribose) polymerase (PARP), caspase 3 and RIPK1 were purchased from Cell Signaling Technology. Horseradish peroxidase (HRP)-conjugated secondary antibodies were obtained from Thermo Fisher Scientific. Cy5-conjugated anti-rabbit secondary antibody was from Jackson ImmunoResearch Laboratories. The hCaf1a antibody was from Abnova. The transfection reagent Lipofectamine™ 2000 was purchased from Invitrogen and Vigofect was from Vigorous. Moloney murine leukemia virus (M-MLV) reverse tanscriptase, hygromycin B and Hoechst 33342 were obtained from Invitrogen. The gastric tumor tissues were kindly gifted by Professor Zhou HM (Tsinghua University) and the description of the tissues has been described elsewhere [35]. Actinomycin D, agarose, ribonuclease A (RNase A), propidium iodide, H_2O_2, hydroxyl urea (HU), cisplatin, Triton X-100, bovine serum albumin (BSA), NaCl and mouse anti-β-actin antibody were purchased from Sigma. Tris, EDTA, dextran sulfate, deionized formamide, formamide, and crystal violet were purchased from Amresco. Sodium deoxycholate, sodium dodecyl sulfate (SDS) and paraformaldehyde were from Merck. RNase inhibitor was from Promega and EvaGreen dye was from Biotium. Fluoromount-G was from Southern Biotechnology Associates. All other chemicals were of analytical grade.

2.2. Cell culture

MKN28 and AGS cell lines were purchased from the China Center of American Type Culture Collection (ATCC, Wuhan, China) and cultured in Dulbecco's modified Eagle's medium (DMEM, Gibco) with 10% FBS (fetal bovine serum, Gibco) at 37 °C with 5% CO_2.

2.3. Establishment of PARN-depleted stable cell line

Stable PARN-depleted cell line was obtained by down-regulation of endogenous PARN expression by shRNA treatment. The oligonucleotides encoding the small hairpin RNA (shRNA) were as follows: 5′-GATCCATCTCGAAGAACAGCCCTGTTCAAGAGACAGGGCTGTTCTTCGAGATGCTTTTTTGGAAA-3′ (sense); and 5′-AGCTTTTCCAAAAAAGCATCTCGAAGAACAGCCCTGTCTCTTGAACAGGGCTGTTCTTCGAGATG-3′ (antisense). The shRNA oligonucleotides were cloned into the linearized vector pSilencer hygro (Ambion). The plasmids were transfected into the MKN28 and AGS cells using Lipofectamine™ 2000 (Invitrogen) according to the instructions of the manufacturer. The pSilencer hygro negative control vector was supplied within the kit (Ambion) and the sequence of the negative control was 5′-GATCCACTACCGTTGTTATAGGTGTTCAAGAGACACCTATAACAACGGTAGTTTTTTGGA-3′. The cells were maintained under a selective culture medium containing hygromycin B with a concentration of 200 μg/ml and 400 μg/ml for the MKN28 and AGS cells, respectively. The stable PARN-knockdown cell lines were obtained after 15–20 day selection. The specificity and knockdown efficiency of PARN were checked by real-time reverse transcription PCR (RT-PCR) and Western blot analysis.

2.4. Real-time RT-PCR

The total RNA was extracted from the cells using a Qiagen RNA extraction kit. In each reaction, 1 μg total RNA was reverse-transcribed into cDNA using the reverse tanscriptase of M-MLV. The obtained cDNA was diluted 2× with Tris–EDTA, and then 1 μl diluted cDNA was analyzed by quantitative PCR using a Stratagene MX3005p cycler and EvaGreen dye with three repetitions. The primers used for PCR were as follows: *PARN* forward, 5′-CGGAATTCGGCGAGTAGAACC-3′; *PARN* reverse, 5′-CCTCCTCTATGGCCTGGTACA-3′; *p21* forward, 5′-GGCGAGGCCGGGATGAGTTG-3′; *p21* reverse, 5′-CTGCCGCCGTTTTCGACCCT-3′; *p27* forward, ′-ATCACAAACCCCTAGAGGGCA-3′; *p27* reverse, 5′-GGGTCTGTAGTAGAACTCGGG-3′; *p53* forward, ′-GAGGTTGGCTCTGACTGTACC-3′; *p53* reverse, 5′-TCCGTCCCAGTAGATTACCAC-3′; *hcaf1a* forward, 5′-AAGGTGGATTACAGGAGGTGG-3′; *hcaf1a* reverse 5′-TGAACCAGAACCAAGGCCATA-3′; *hcaf1b* forward, 5′-AGATCCGAGAAATCGTGCTCA-3′; *hcaf1b* reverse, 5′-ATTGCACCGCAGAAGCTGATA-3′; *hccr4a* forward, 5′-TACCCGCAGAACTCGGAAAC-3′; *hccr4a* reverse, 5′-CAGCAGCCGTCTTGTTCCAT-3′; *hccr4b* forward, 5′-CTGCCGTCAGCATCATTCAC-3′; *hccr4b* reverse, 5′-TCCATCATATCCACGCTCCTT-3′; *hccr4d* forward, 5′-CTACACCGTGGGAGAATCTGC-3′; *hccr4d* reverse, 5′-GATGTCTGGCTC

AGGTTGTCA-3′; *PAN2* forward, 5′-ACCCAAGTCTGCTACAGAATGT-3′; *PAN2* reverse, 5′-CACGCTGTGCAATTCAGAGTA-3′; *PAN3* forward, 5′-GGATGGAGGTGCTTTAACTGA-3′; *PAN3* reverse, 5′-GATCATGGGCTGAA TATGGCTT-3′; *GAPDH* forward, 5′-CGCTCTCTGCTCCTCCTGTT-3′; *GAPDH* reverse, 5′-CCATGGTGTCTGAGCGATGT-3′; *18S rRNA* forward, 5′-CAGCCACCCGAGATTGAGCA-3′ and *18S rRNA* reverse, 5′-TAGTAGCG ACGGGCGGTGTG-3′.

2.5. Western blotting

Whole cell lysates were prepared in RIPA buffer (50 mM Tris pH 8.0, 150 mM NaCl, 1% Triton X-100, 1 mM EDTA, 0.5% sodium deoxycholate and 0.1% SDS). The lysates (40 μg) were boiled in 5× protein loading buffer, separated by a 12.5% SDS-PAGE and transferred to a PVDF membrane (GE). Bound primary antibodies were detected with HRP-conjugated secondary antibodies (1:3000 dilution) using SuperSignal West Pico Chemiluminescent Substrate (Thermo Fisher Scientific).

2.6. Cell proliferation assay

Cell proliferation was evaluated by the 3-(4,5-dimethylthiazol-2-yl)-5-(3-carboxymethoxyphenyl)-2-(4-sulfophenyl)-2H-tetrazolium, inner salt (MTS) assay and the AlamarBlue assay. As for the MTS assay, cell proliferation rates were determined using the CellTiter 96 Aqueous One Solution Proliferation Assay Kit (Promega). The PARN-depletion stable cell lines were seeded into 96-well culture plates with a density of 1×10^3 cells/well. After cultivation for 0, 1, 2, 3, 4 and 5 days, the MTS solution was added to the medium and the cells were incubated for another 1 h. Cell viability was determined by measuring the absorbance at 490 nm using a microplate reader (Bio-Rad). For the AlamarBlue assay, MKN28 and AGS stable cells (2×10^3 cells/well) were seeded in 96-well plate. After 24 h cultivation, the cells were moved to 100 μl fresh culture medium and then 10 μl alamar blue (Invitrogen) was added to each well. After 4 h incubation with the dye, cell viability was analyzed by detecting the fluorescence emitted at 585 nm after excited at 570 nm on a multiwell plate reader (FLUOstar Omega).

2.7. Colony formation assay

Cells (1×10^3) were seeded in 10-cm dishes. The culturing medium containing hygromycin B was replaced every 3–4 days. After being seeded for 2 weeks, cells were stained with 0.1% crystal violet and then photographed. The soft agar assay was performed in 6-well plates. Cells (1×10^4) were resuspended in the DMEM medium with 0.7% agarose (Sigma-Aldrich) and seeded onto 6-well plates, which had been precoated with 1% base agarose. Cells were cultured for 2 weeks and then stained with 0.005% crystal violet.

2.8. Cell cycle assay

Cells were fixed with 70% ethanol at 4 °C overnight. After washing with PBS, cells were incubated with RNase A (100 μg/ml) in PBS for 30 min at 37 °C and then stained with propidium iodide (50 μg/ml). The percentages of cells in the G_0/G_1, S and G_2/M phases of the cell cycle were determined by FACSCalibur (BD Biosciences) and analyzed with ModFit LT 3.0.

2.9. Cell apoptosis assay

Cells at 90% confluence were exposed to UV light or treated with hydrogen peroxide (H_2O_2), hydroxyl urea (HU) and cisplatin. After treatment, the cells were harvested, rinsed in PBS and resuspended in annexin V binding buffer. Then the cells were incubated with propidium iodide (PI) and FITC-labeled annexin V (BD Biosciences) according to the manufacturer's instructions. Apoptosis analysis was carried out on a FACSCalibur flow cytometer (BD Biosciences).

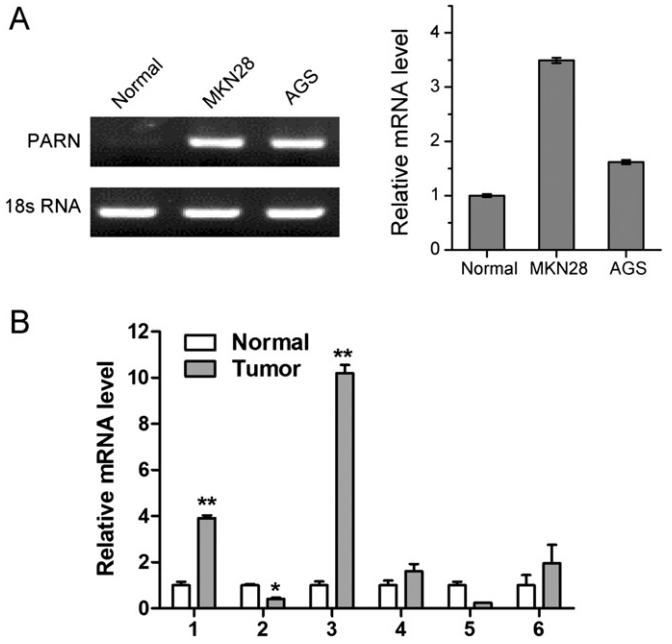

Fig. 1. Upregulation of *PARN* in human gastric cancer cell lines and tumor tissue samples. (A) Relative mRNA level of *PARN* in the MKN28 and AGS human gastric cancer cell lines by semi-quantitative RT-PCR (left) and quantitative real-time PCR analysis (right). The normal stomach tissue was used as a control. The abundance of *PARN* mRNA by real-time RT-PCR was quantified by the *GAPDH* mRNA and normalized by the value of the control. (B) Real-time RT-PCR analysis of *PARN* mRNA expression in six pairs of human gastric tumor tissue samples. The abundance of *PARN* was quantified by the *GAPDH* mRNA and normalized by the value of the normal tissue in each pair of sample. The error bars are standard deviations from three repetitions of the total RNA samples from one patient ($^*p < 0.05$, $^{**}p < 0.01$).

2.10. Cell motility assays

The cell motility was assessed by wound healing, transwell and invasion assays. As for the wound healing assays, cells were seeded in 6-well plates and cultured until they approached confluence. The monolayer was scratched with a 200 μl pipette tip. After 0, 24 and 48 h cultivation, the cultures were imaged by an Olympus IX71 inverted microscope and the wound size was measured. Transwell migration assay was performed by suspending 5×10^4 cells in serum-free DMEM and plated on 24-well Millicell chambers (8-μm pore size, Millipore) without matrigel coating. Invasion assay was performed by adding 5×10^5 cells in serum-free DMEM to the upper chamber, which was precoated with 5 mg/ml matrigel (Vigorous). Then the medium containing 10% FBS was added to the lower chamber as a chemoattractant for both the transwell and invasion assays. After 24 h cultivation, cells in the upper chamber were removed with a cotton swab and then stained with 0.5% crystal violet. The migration and invasion ability of the cells were determined by dissolving the stained cells with 10% acetic acid and measuring the absorbance at 560 nm.

2.11. Immunofluorescence microscopy

The MKN28 and AGS cells were grown on glass coverslips. After 20 h incubation, cells were fixed in 4% paraformaldehyde for 30 min, followed by a 30 min permeabilization in 0.2% Triton X-100 in PBS. Then the cells were blocked in PBS containing 10% goat serum for 1 h at ambient temperature. Immunostaining was carried out using Dcp1a (Abcam) primary antibodies at 4 °C overnight, washed three times with PBS and incubated with the Cy5-conjugated anti-rabbit secondary antibody (Jackson ImmunoResearch Laboratories) for 1 h at room temperature. The nuclei were counterstained with Hoechst 33342 (Invitrogen) for 1 min and rinsed with PBS. The cells were mounted using Fluoromount-G (Southern

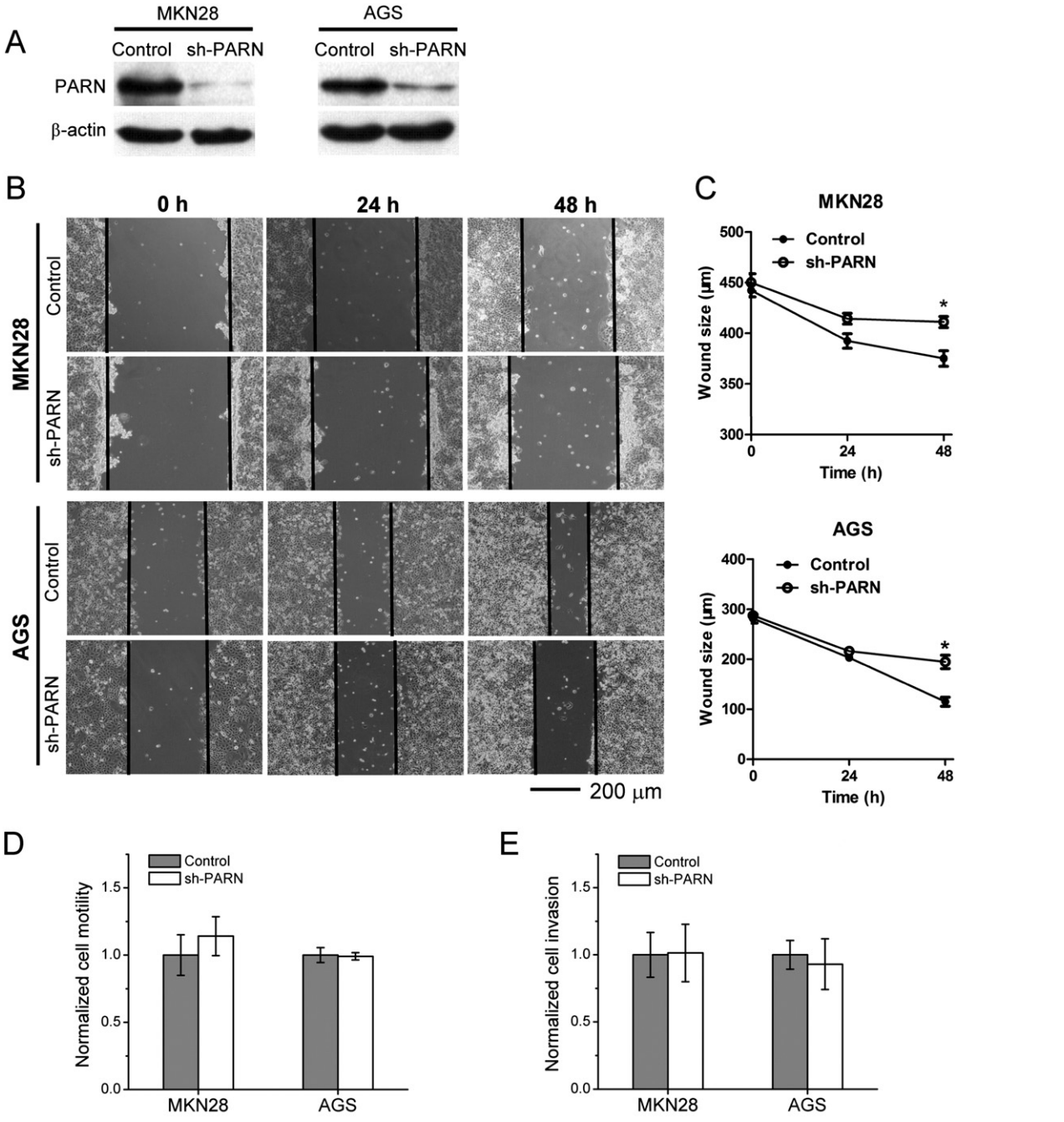

Fig. 2. Effect of PARN-knockdown on cell motility. (A) Western blot analysis of the knockdown efficiency in the stable MKN28 and AGS cell lines used for further analysis. β-Actin was used as an internal control of protein loading. (B) Effect of PARN-depletion on cell motility by wound healing assay. MKN28 (top) and AGS (bottom) cells were grown to 90% confluency and scratched with a pipette tip. The initial wound sizes were different for MKN28 and AGS cells because that MKN28 cells were prone to grow into clusters. To ensure the repeatability of the experiments, the initial wound size of MKN28 cells was larger than that of AGS cells. After scratch, the sizes of the wounds were determined after 24 h and 48 h incubation. (C) Quantification of the changes of wound size along with incubation time. Data are mean ± SD of three independent experiments. $^*p < 0.05$. (D) PARN-depletion does not affect cell motility monitored by transwell assay. MKN28 and AGS cells (5×10^4) were plated on 24-well Millicell chambers without coating by matrigel. After 24 h cultivation, the cell motility was determined by dissolving the crystal violet stained cells with 10% acetic acid and measuring the absorbance at 560 nm. The data of the PARN-depleted cells were normalized by those of the control cells. Relative quantification data are mean ± SD of three independent experiments. (E) PARN-depletion does not affect cell invasion ability. The cells (5×10^5) were plated on 24-well Millicell chambers precoated with 5 mg/ml matrigel. After 24 h cultivation, the cell invasiveness was determined by dissolving the crystal violet stained cells with 10% acetic acid and measuring the absorbance at 560 nm. The data of the PARN-depleted cells were normalized by those of the control cells. Relative quantification data are mean ± SD of three independent experiments. No significant difference was observed for the results of the transwell and invasion assays ($p > 0.2$).

Biotechnology Associates) and analyzed by a Carl Zeiss LSM 710 confocal microscope.

2.12. RNA fluorescence in situ hybridization

Poly(A)$^+$ RNAs were visualized by fluorescent in situ hybridization (FISH) as described previously [36]. In brief, cells were seeded on glass coverslips for 24 h, fixed with 4% paraformaldehyde in PBS and denatured in 70% formamide at 70 °C. The cells were permeabilized and blocked for 40 min by 0.5% Triton X-100/2% BSA in PBS, followed by 2 h of prehybridization at ambient temperature in hybridization buffer (4 × SSC, 5% dextran sulfate, 2% BSA, 35% deionized formamide and 10 U RNase inhibitor). Hybridization was carried out overnight at ambient temperature in a humidified dark chamber in the presence of 300 ng/ml

Cy5-conjugated oligo(dT)$_{30}$ probe in hybridization buffer. After washing with 4 × SSC and 35% deionized formamide for three times, the cells were counterstained with Hoechst 33342 (Invitrogen) and mounted with Fluoromount-G. Immunofluorescence images were obtained by a Carl Zeiss LSM 710 confocal microscope.

2.13. Luciferase reporter assay

The luciferase reporter assay was performed as described previously [21]. In brief, cells were seeded into 24-well plates before transfected with the *p21* promoter, 5′-UTR or 3′-UTR luciferase reporter constructs. pRL-TK was used as an internal control. After transfected for 24 h, the luciferase activity was measured using the dual luciferase kit (Vigorous) according to the manufacturer's protocol.

2.14. Bioinformatics analysis

The ONCOMINE database (https://www.oncomine.org/resource/login.html), a cancer microarray database and online data-mining platform [37], was used to search for the changes of PARN mRNA level in various types of cancers including gastric cancer. The bioinformatics analysis was performed using a threshold (p-value) of 1×10^{-4}, a threshold (fold change) of 1.5 and a data type of mRNA. There are 9 datasets with PARN mRNA levels in gastric cancers, and all of the 9 datasets were used for the analysis.

2.15. mRNA stability assay

For the mRNA stability measurement, MKN28 and AGS cells were cultured in 12-well plates in the DMEM medium. Transcription inhibition was accomplished by addition of 5 μg actinomycin D for 0, 2, 4, 6, 8, 10 or 12 h. After treatment, the total RNA was extracted by standard procedures. Then the amount of *p21*, *p27* or *p53* mRNA was determined by real time RT-PCR by using *GAPDH* as an internal control. The data were normalized by the untreated sample. To avoid misleading results caused by the toxic effect of long-term actinomycin D treatment, mRNA half-life was determined only for those mRNAs with a significant decrease within 4 h of actinomycin D treatment. The half-life of mRNAs was obtained by fitting the time-course data using the first-order exponential decay kinetics.

2.16. Quantification and statistical analysis

Relative quantification was estimated by comparing the PARN-depleted cells with the control cells cultivated under the same conditions and normalizing the data of the PARN-depleted group by the control group in each biological replicate. Most cell experiments were performed and analyzed with at least three independent biological replicates, which were performed separately using different sets of cells. The MTS assay, AlamarBlue assay, colony formation assay and quantitative PCR experiments were performed with at least two biological replicates. To avoid the misleading statistical analysis caused by large errors between different sample preparations, the presented data of these assays were from one biological replicate with at least three repetitions. Statistical analysis was performed using GraphPad Prism 5. The unpaired two-tailed Student's t test was used to compare the sets of data with at least three repetitions by assuming a Gaussian distribution. A p value less than 0.05 was considered significant.

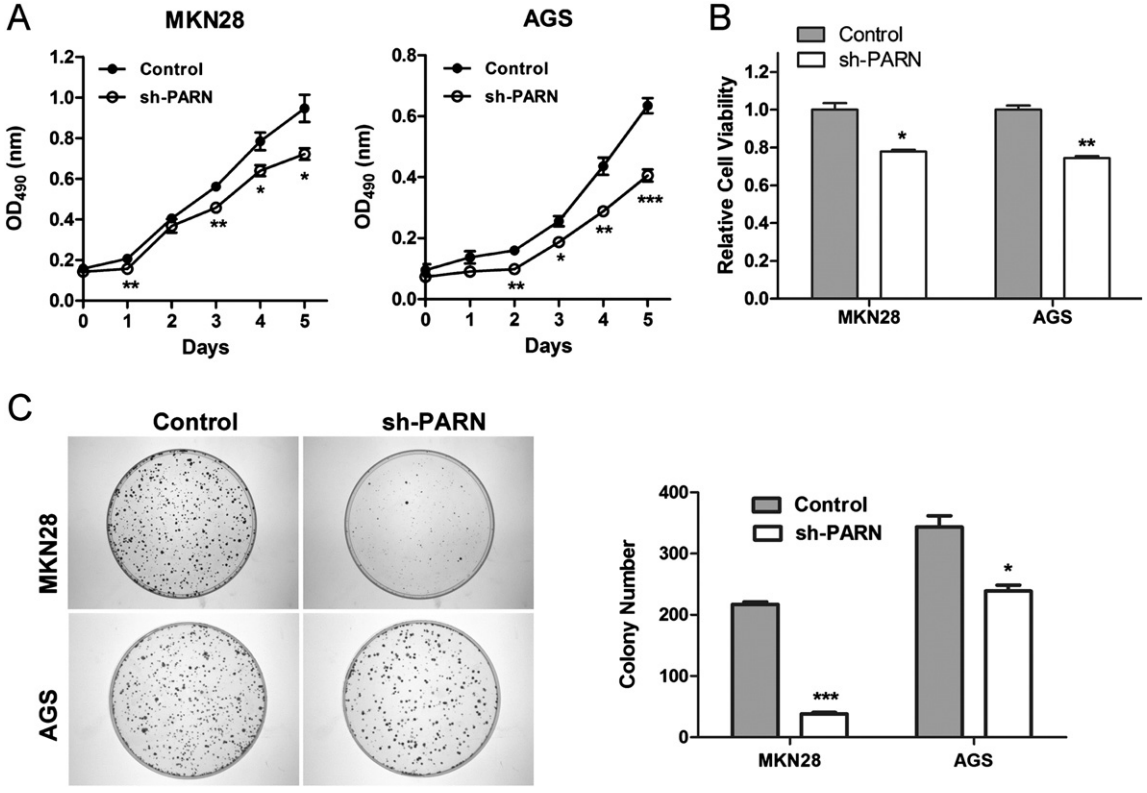

Fig. 3. Depletion of PARN inhibits cell proliferation. (A) Cell proliferation monitored by the MTS assay. The MKN28 and AGS cells were cultured in the DMEM medium with the addition of either 200 μg/ml (MKN28) or 400 μg/ml (AGS) hygromycin B. The growth curves for MKN28 and AGS cells were determined by MTS assay. (B) Cell viability detected by the AlamarBlue assay. MKN28 and AGS cells (2×10^3 cells/well) cultivated for 24 h and then treated with 10 μl alamar blue. The fluorescence at 585 nm was measured after 4 h incubation. The data of the PARN-depleted cells were normalized by those of the control cells. (C) Colony formation assay. The MKN28 and AGS cells (1×10^3) were cultured in the DMEM medium containing 200 μg/ml (MKN28) or 400 μg/ml (AGS) hygromycin B for 2 weeks and then stained with crystal violet. The number of colonies was counted. All presented data in Fig. 3 are mean ± SD of three repetitions of one of the biological replicates and all assays were verified using at least one different biological replicate. *$p < 0.05$, **$p < 0.01$, and ***$p < 0.001$.

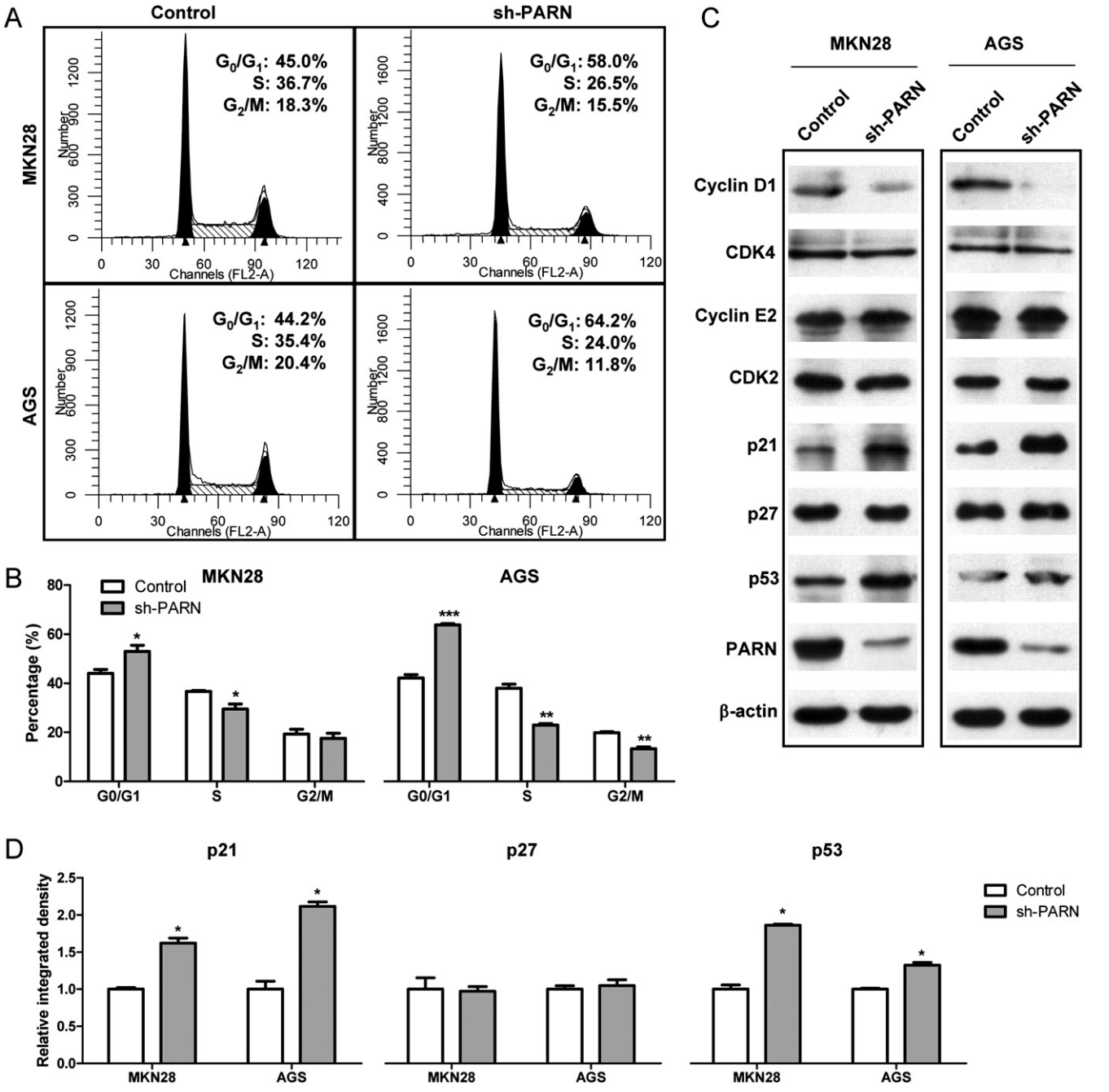

Fig. 4. Depletion of PARN induces cell cycle arrest at the G_0/G_1 phase. (A) Representative profiles of cell cycle progression analyzed by flow cytometry using propidium iodide staining. The DNA contents of the control and PARN-knockdown cells were measured by propidium iodide staining and sorted by flow cytometry. (B) Percentages of cells in the G_0/G_1, S and G_2/M phases. The percentage of each phase was quantified from the flow cytometry analysis of 20,000 cells. (C) Effect of PARN-depletion on the expression of cell cycle-related proteins. Western blot analysis was performed for the cell lysates prepared from the control and PARN-depleted cells. The proteins were identified and quantified by antibodies against cyclin D1, CDK4, cyclin E2, CDK2, p21, p27, p53 and PARN. β-Actin was used as an internal control for protein loading of Western blotting. (D) Quantitative analysis of the protein expression changes of p21, p27 and p53. The quantification of cyclin D1, cyclin E2, PARN, CDK2 and CDK4 are shown in Supplemental Fig. S4. Quantitative data in panels B and D are mean ± SD of three independent biological replicates. $^{*}p < 0.05$, $^{**}p < 0.01$.

3. Results

3.1. Expression level of PARN in human gastric cancer cells and tissues

Previous studies have shown that PARN has a high expression level in acute leukemia [34] and has been proposed to be a potential cancer therapeutic target [7]. To examine the expression status of PARN in human gastric cancer, semi-quantitative and real-time RT-PCR was used to examine the mRNA level of *PARN* in two human gastric cancer cell lines and six pairs of gastric tumor tissues from patients described elsewhere [35]. The results (Fig. 1) indicated that *PARN* was upregulated in both of the two gastric cancer cell lines. Meanwhile, significantly elevated *PARN* expression was found in two tumor samples (#1 and #3) among the six pairs of tissue samples, while *PARN* downregulation was also observed in sample #2. We further analyzed the changes of *PARN* expression in various cancers via the online cancer microarray database ONCOMINE [37]. PARN was found to be upregulated in many types of cancers (Supplemental Fig. S1). Particularly, upregulation of *PARN* mRNA level was found in 5 out of 9 datasets of gastric cancers.

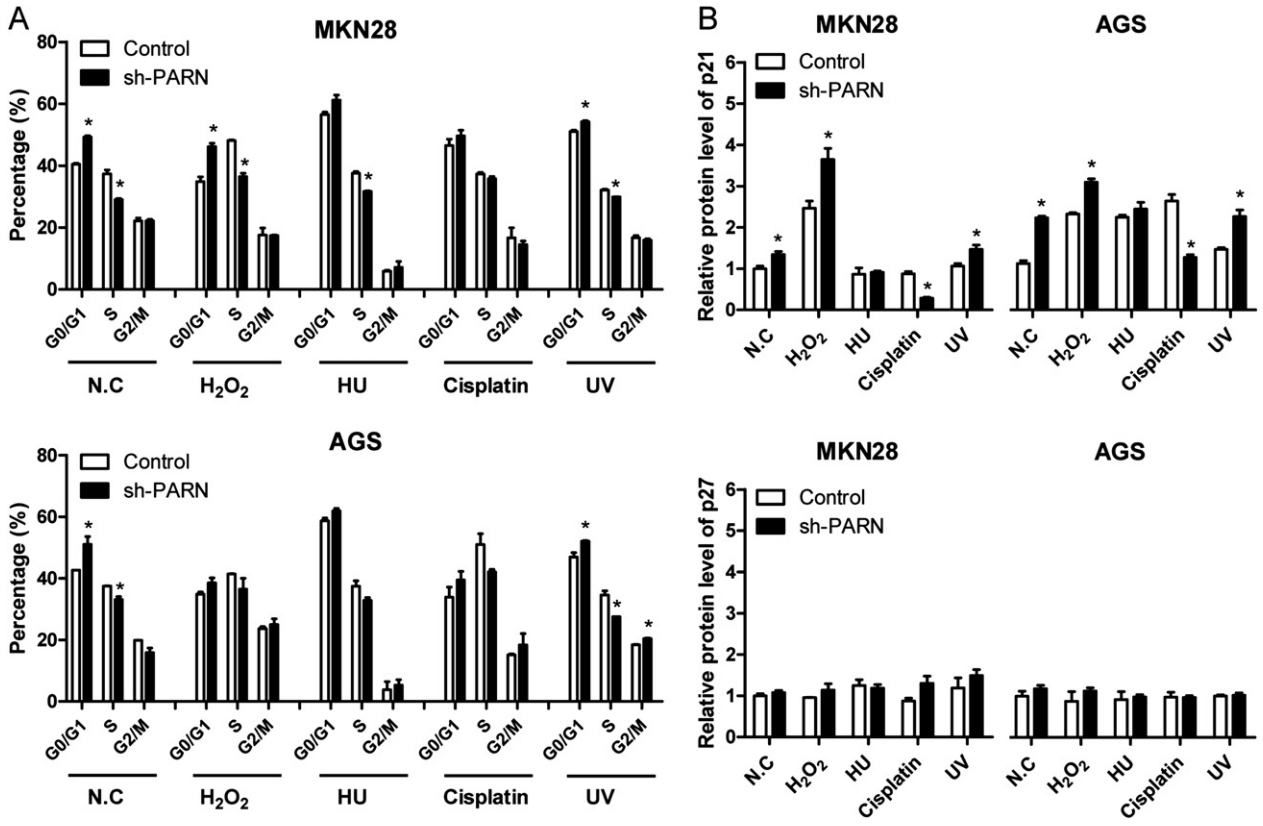

Fig. 5. Effect of DNA-damaging treatments on cell cycle arrest induced by PARN-depletion. (A) Percentages of cells in the G_0/G_1, S and G_2/M phases quantified by three flow cytometry analysis of 20,000 cells. Representative profiles are presented in Supplemental Fig. S6. (B) Expression levels of p21 (top) and p27 (bottom) by Western blot analysis. Representative Western blot results are shown in Supplemental Fig. S7. MKN28 and AGS cells at 90% confluence were exposed to UV light or treated with the DNA-damaging reagents and then the cells were harvested. The whole cell lysates were used for Western blot analysis using the antibodies against p21 and p27. β-Actin was used as a loading control. Data are mean ± SD of three independent experiments.

3.2. PARN-depletion inhibits cell proliferation

To investigate the potential roles of PARN in tumorigenesis, stable cell lines with the depletion of endogenous PARN were achieved by shRNA-mediated knockdown in MKN28 and AGS cells. Five clones in MKN28 cells and six clones in AGS cells were obtained, and the knockdown efficiencies were checked by real-time RT-PCR and Western blotting (Supplemental Fig. S2). The clones with >80% knockdown efficiency at both the mRNA and protein levels were selected for further research (Fig. 2A).

Previously PARN-knockdown has been shown to increase the motility of mouse C2C12 myoblasts by modifying the fates of mRNAs required for cell migration and adhesion [33]. Thus the effect of PARN-knockdown in the gastric cancer cells was first investigated by the wound-healing assay (Fig. 2B). The size of the wound was measured at 24 h and 48 h after the monolayer of cells was scratched (Fig. 2C). The migration rates of both MKN28 and AGS cells were inhibited by the depletion of PARN after 48 h incubation, but the difference was minor for cells incubated 24 h after scratching. Meanwhile, the results from both transwell and invasion assays indicated that the knockdown of PARN did not influence the migration and invasion rates of the gastric cancer cells (Fig. 2D and E). Thus the decrease in wound healing rate by PARN-knockdown observed at 48 h was more likely to be caused by the difference in cell proliferation but not cell motility. Moreover, the differential effect of PARN-knockdown observed in mouse myoblasts and gastric cancer cells also suggested that cancer cells might utilize different regulatory mechanisms of cell motility from mouse myoblasts/normal cells.

The effect of PARN-knockdown on cell proliferation was examined by MTS assay, AlamarBlue assay and colony formation experiments. The time-course study by MTS assay indicated that the depletion of PARN significantly retarded cell proliferation after 2–3 day incubation for both of MKN28 and AGS cells (Fig. 3A). Meanwhile, AlamarBlue assay also indicated that the cell viability was significantly inhibited by PARN-knockdown after 24 h cultivation (Fig. 3B). Consistently, severe reduction of proliferation rate induced by PARN-depletion was also observed by colony formation experiments for both types of cells (Fig. 3C). We failed to form colony by MKN28 cells in soft agar. Nonetheless, the soft agar assay of AGS cells confirmed that PARN-depletion resulted in an inhibitory effect on the colony formation ability (Supplemental Fig. S3).

3.3. PARN depletion leads to cell cycle arrest by upregulating p21 expression

To investigate the mechanism underlying the inhibitory effect of PARN-depletion on cell proliferation, cell cycle progression was analyzed by flow cytometry using propidium iodide (PI) staining (Fig. 4A and B). For both gastric cancer cell lines, the depletion of PARN induced a significant elevation in the proportion of G_0/G_1 phase cells (9% and 22% increase in MKN28 and AGS cells, respectively) accompanied with a reduction in the amount of S phase cells (7% and 15% decrease in MKN28 and AGS cells, respectively). The effect of PARN-depletion on cell populations at the G_2/M phase was minor and the difference might be caused by the indirect effect of arresting cells at the G_0/G_1 phase. These observations suggested that PARN might involve in cell cycle regulation and the depletion of PARN inhibited cell cycle progression by retarding the phase transition from G_0/G_1 to S.

The arrest of the cells at the G_0/G_1 phase was confirmed by the significant decrease in the amount of the G_1/S-specific cyclin D1, while

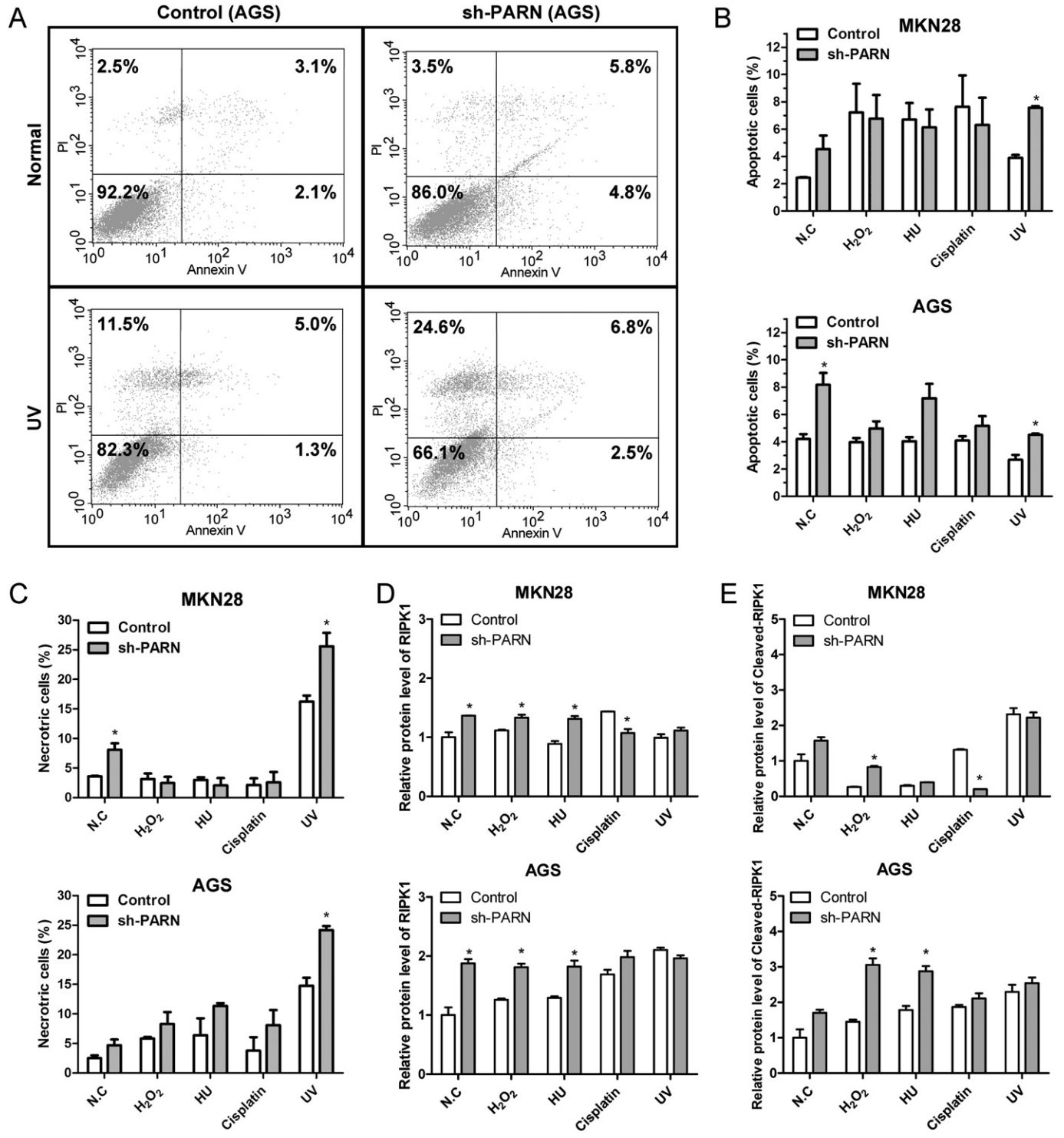

Fig. 6. PARN-depletion promotes cell death. (A) Representative profiles of AGS cell death determined by annexin V binding (horizontal) and PI exclusion (vertical) followed by flow cytometry. The profiles of the MKN28 and AGS cells treated by various DNA-damaging reagents are shown in Supplemental Fig. S8. (B) Percentages of apoptotic MKN28 and AGS cells qualified from the annexin V-positive populations. (C) Percentage of necrotic cells qualified from the PI-positive and annexin V-negative populations. The cells are treated with various DNA-damaging reagents and UV irradiation. N.C. represents cells without any treatment. The percentages of apoptotic and necrotic cells were quantified from 10,000 cells. (D) Changes in RIPK1 expression. (E) Changes in the amounts of cleaved RIPK1. Representative Western blot analysis of the changes in the expression of PARP, caspase 3 and RIPK1 is shown in Supplemental Fig. S9. No significant changes were found for PARP and caspase 3 expression levels. Data are mean ± SD of three independent experiments. $^{*}p < 0.05$.

the other cell cycle promotion factors were not affected by the depletion of PARN (Fig. 4C and Supplemental Fig. S4). It is worth noting that the function of cyclin E can rescue many of the phenotypes of cyclin D1-deficient mice [38]. As shown in Fig. 4C, the level of cyclin E2 was unaffected by PARN-knockdown, implying that the down-regulation of cyclin D1 might not be the predominant cause of the growth inhibition effect of PARN-depletion. Thus the expression levels of the major negative regulators of the G_1–S transition (p53, p21 and p27) were examined by Western blotting in PARN-depleted MKN28 and AGS cells (Fig. 4C and D). The results indicated that knockdown of PARN led to a

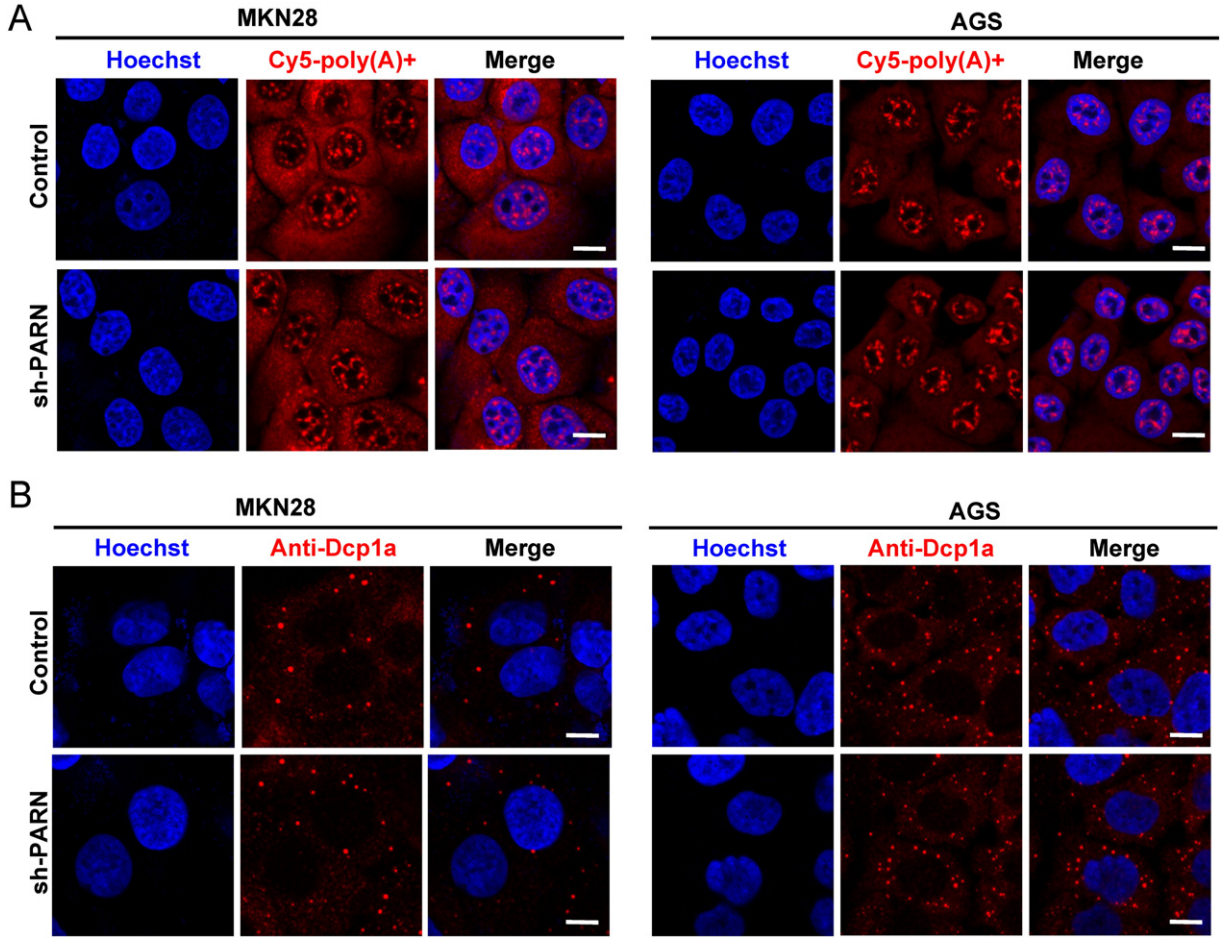

Fig. 7. PARN-depletion did not affect the formation of intracellular poly(A)$^+$ foci. (A) Formation of poly(A)$^+$ RNA granules detected by FISH. The poly(A)$^+$ RNAs were hybridized with Cy5-conjugated oligo-$(dT)_{30}$ in the control and PARN-depleted MKN28 and AGS stable cells. The nuclei were counterstained with Hoechst 333242. After staining, the cells were visualized and analyzed by immunofluorescence confocal microscopy. (B) Formation of cytoplasmic P-bodies. Dcp1a was used as the marker protein of P-body. Quantification analysis of the numbers of P-bodies in the cells is shown in Supplemental Fig. S10. The scale bar represents 10 μm.

significant upregulation of p21 and p53 proteins, but no changes in p27 expression for both cell lines (Fig. 4C and D). Thus the phonotype in PARN-depleted MKN28 and AGS cells was more likely to be caused by the accumulation of p53 and the CDK inhibitor p21. Moreover, upregulation of p21 expression was observed for all PARN-depleted stable cell lines grown from various clones with >80% knockdown efficiency (Supplemental Fig. S5).

We further investigated whether the effect of PARN-depletion on cell cycle progression was affected under DNA-damaging conditions (Fig. 5 and Supplemental Fig. S7). The DNA-damaging treatments influenced the cell cycle progression differentially. Depletion of PARN could arrest MKN28 cells at the G_0/G_1 phase for most DNA-damaging treatments except for cells treated by cisplatin. As for AGS cells, PARN-depletion induced cell-cycle-arrest was retained only for UV treatment. For the control cells, p21 upregulation by most DNA-damaging treatments was pronounced in AGS cells, while minor in the MKN28 cells. Nonetheless, PARN-depletion led to similar patterns of changes in p21 and p27 expression in the two cell lines when treated by various DNA-damaging reagents or UV. In detail, the expression level of p27 was unaffected by stress conditions as well as PARN-depletion (Fig. 6B). Meanwhile, PARN-depletion induced upregulation of p21 was found for cells treated by H_2O_2 and UV. No significant effect of PARN-depletion was observed for cells treated by HU. Surprisingly, treatment by cisplatin, one of the most potent chemotherapy drugs widely used for cancer treatment, reversed the effect of PARN-depletion-induced increase of p21 expression. Furthermore, our results suggested that the effect of cisplatin as well as cancer therapy of *p21*-gene transfer with cisplatin might be unsatisfactory in PARN-depleted tumors. Further research is needed to elucidate the underlying mechanism of this surprising observation.

Fig. 8. Changes in the mRNA level and stability of *p21*, *p27* and *p53* induced by PARN-depletion. (A) Steady-state mRNA levels of *p21* (left), *p27* (middle) and *p53* (right) determined by real time RT-PCR ($n = 3$). (B) mRNA stability of *p21* (left), *p27* (middle) and *p53* (right). mRNA stability was determined by treating the MKN28 and AGS cells by actinomycin D with a concentration of 5 μg/ml. Then the changes in the mRNA levels of *p53* and *p21* were obtained by real-time RT-PCR analysis at various time intervals ($n = 3$). The data of mRNA with a fast decay within 4 h of actinomycin D treatment were fitted by the first-order exponential decay kinetics and the fitted data are shown as solid lines. The changes in mRNA amounts after 4 h of actinomycin D treatment might be affected by alterations in cellular physiology and thus were not used for fitting. The half life of *p21* in control AGS cells was 1.1 ± 0.1 h, while those in the other groups were >4 h. The half lives of *p27* were 0.7 ± 0.4 h, 1.4 ± 0.2 h, 0.9 ± 0.2 h and 1.2 ± 0.2 h for the control MKN28 cells, the PARN-depleted MKN28 cells, the control AGS cells and the PARN-depleted AGS cells, respectively. No significant difference was observed for the fitted half-lives of *p27* among groups ($p = 0.21$), and the best fitted half-life of *p27* was 1.1 ± 0.2 h for all groups. (C) Effect of PARN-depletion on the mRNA levels of the other deadenylases determined by real time RT-PCR ($n = 3$). (D) Effect of PARN-depletion on the protein levels of human Caf1a and Ccr4a. The protein levels of the other deadenylases were not checked due to the lack of highly specific antibodies. (E) Effect of PARN-depletion on *p21* promoter-driven luciferase reporter activity ($n = 8$). MKN28 and AGS cells were transfected with *p21* promoter-driven luciferase reporter constructs. The measured luciferase activity was normalized by the activity of *Renilla* luciferase. (F) Effect of PARN-depletion on *p21* 5′- and 3′-UTR luciferase reporter activity ($n = 3$). MKN28 and AGS cells were transfected with pGL3-basic vector, *p21* 5′-UTR or *p21* 3′-UTR luciferase constructs. pRL-TK was co-transfected and used as an internal control. Luciferase reporter activities were measured and expressed as ratios of firefly luciferase to *Renilla* luciferase. Quantitative data are mean ± SD of at least three repetitions from one of the biological replicates. $^*p < 0.05$, $^{**}p < 0.01$, and $^{***}p < 0.001$.

3.4. PARN-depletion promotes cell death

The above results showed that the PARN-depletion cells were arrested at the G_0/G_1 phase probably via upregulation of p53 and p21. Both p53 and p21 are key regulators in cell growth and survival. The arrested cells generally have two distinct fates: returning back to the cell cycle or initiating cell death pathways. The effect of PARN-knockdown on cell death was analyzed by bivariate flow cytometry using annexin V and PI staining. PI stains the necrotric cells, while annexin V stains the apoptotic cells [39]. Thus the cells separated by flow cytometry can be divided into four populations of PI-negative and annexin V-negative, PI-positive and annexin V-negative, PI-negative and annexin V-positive as well as PI-positive and annexin V-positive cells, which corresponds to normal cells, primary necrotric

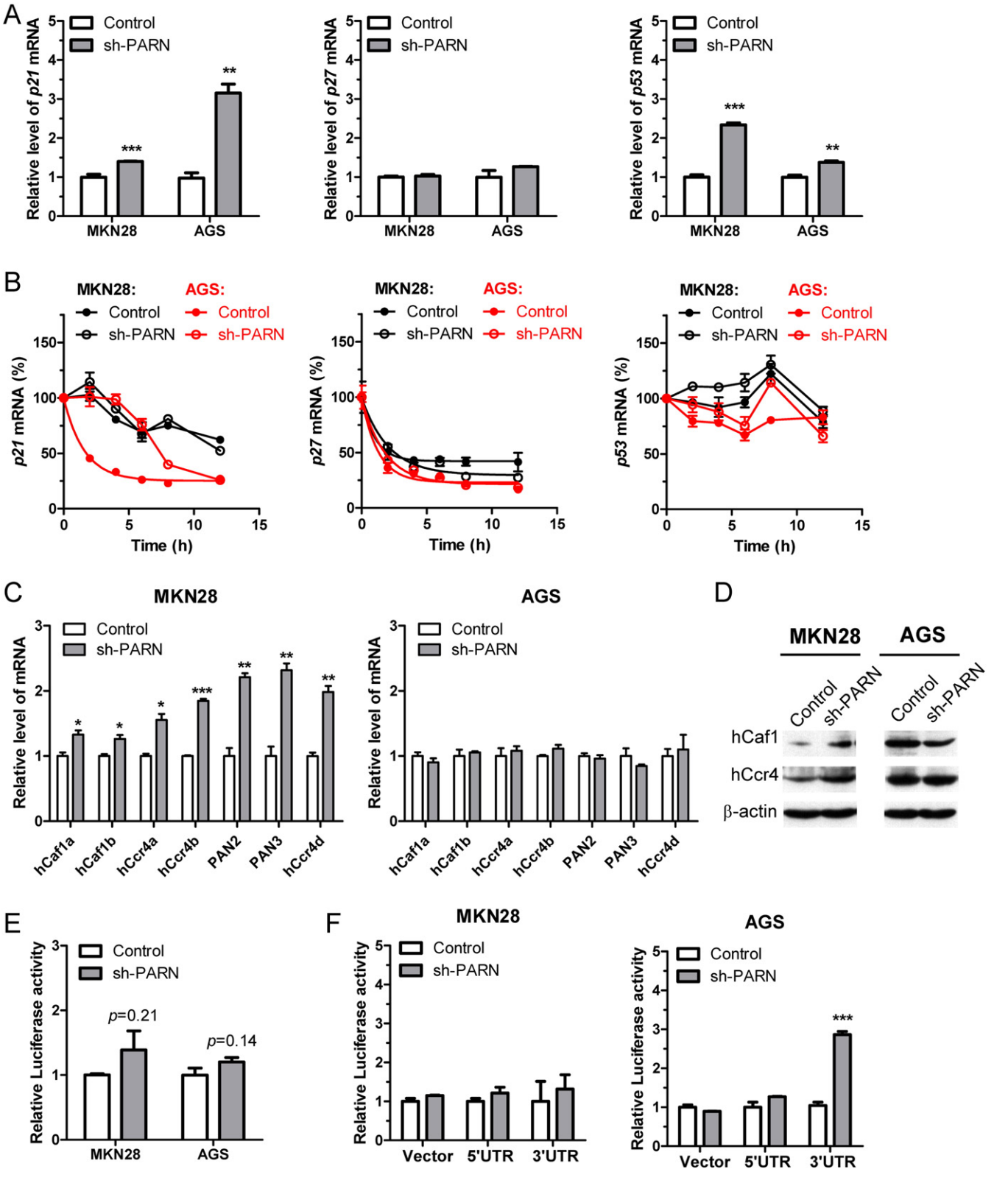

cells, late apoptotic/secondary necrotric cells and early apoptotic cells, respectively. The results shown in Fig. 6A indicated that the depletion of PARN led to an about two-fold increase in the average values of both annexin V-positive apoptotic cells and PI-positive necrotric cells for both cell lines.

Although cell death was promoted by PARN-depletion in both of the gastric cancer cell lines, the results were not so pronounced due to the limited numbers of apoptotic and necrotric cells. Thus we further investigated whether the effect of PARN-depletion on cell death could be amplified under DNA-damaging conditions studied by bivariate flow cytometry (Supplemental Fig. S8). As shown in Fig. 6B and C, the DNA-damaging reagents affected the two types of gastric cancer cell lines differentially. DNA-damage promoted apoptosis in MKN28 cells, while increased necrosis in AGS cells. Nonetheless, no significant difference in apoptosis and necrosis was observed between the control and PARN-depleted cells, implying that the cell-death promoting effect of PARN-depletion might be neutralized by these DNA-damaging agents. Under UV treatment, a significant increase was induced by PARN-depletion for both of the annexin V-positive and PI-positive populations. However, the two-fold increase was at the same level as the impact of PARN-depletion on untreated cells, implying that the stress conditions did not significantly affect cell death induced by PARN-depletion in the two gastric cancer cells.

No detectable cleavage of PARP and caspase 3 was found in both gastric cell lines under various DNA-damaging treatments, while the expression of RIPK1 was upregulated by PARN-depletion (Supplemental Fig. S9). Upregulation of RIPK1 induced by PARN-depletion was more pronounced in AGS cells than in the MKN28 cells. Moreover, the amount of RIPK1 in PARN-depleted cells was unaffected by DNA damage, but increased in the control cells (Fig. 6D). Only a small portion (<10%) of RIPK1 was cleaved and quite dissimilar effects of DNA damage and PARN-depletion was observed for the two gastric cell lines (Fig. 6E). In AGS cells, the behavior of the cleaved RIPK1 were similar to uncleaved RIPK1, which might be caused by the increase of RIPK1 expression induced by DNA damage and PARN-depletion. Thus the increased cell death caused by PARN-depletion was at least partially via the RIPK1-mediated pathway.

3.5. PARN-depletion does not affect the formation of RNA granules

The translational-repressed or degradable mRNAs may accumulate into cellular foci (RNA granules) that can be stained by RNA probes [40]. Although the behavior of PARN has not been investigated in the formation of the well-characterized cytoplasmic RNA granules, the processing body (P-body) and stress granule, PARN has been shown to be a component of exosome [27]. To assess whether PARN-depletion affected the formation of RNA granules globally, the distribution of poly(A)$^+$ RNAs was visualized by FISH using a fluorescent Cy5-oligo(dT)$_{30}$ probe. For both gastric cancer cells, most of the poly(A)$^+$ foci were found in the nucleus, while a minor amount could also be identified in the cytoplasm of MKN28 cells. A comparison between the control and PARN-depleted cells (Fig. 7A) indicated that the knockdown of PARN did not affect the formation of various poly(A)$^+$ foci. Specifically, the P-bodies, which are proposed to be cytoplasmic sites of mRNA decay, were stained by a P-body marker protein, Dcp1a [41]. Both types of cells possessed considerable amounts of P-bodies, while AGS cells contained even more (Fig. 7B). Neither the number nor the size of the P-bodies was affected by the depletion of PARN (Supplemental Fig. S10). These observations suggested that PARN contributed little to the RNA granule formation in the gastric cancer cells.

3.6. PARN-depletion stabilizes the p21 mRNA

The results in Fig. 4 indicated that the expression levels of p53 and p21 were significantly increased in the PARN-depleted gastric cancer cells. The effect of PARN-depletion on the mRNA levels of *p53*, *p27* and *p21* was investigated by real-time PCR analysis (Fig. 8A). Consistent with the results at the protein level, no significant changes were observed for the abundance of the *p27* mRNA, while both of *p53* and *p21* were upregulated by PARN-depletion. The upregulation of *p53* in MKN28 cells was more pronounced than that in AGS cells, while that of *p21* was higher in AGS cells. The time-course studies were achieved by blocking transcription by actinomycin D and then measuring the residual mRNA level at a given time. Surprisingly, the *p53* transcripts maintained at a high level after treated for 12 h in both cell lines (Fig. 8B). Unlike *p53*, the *p27* transcripts were degraded quickly with a half-life of less than 1 h and PARN-depletion had no impact on the decay of *p27* in both gastric cancer cell lines. The *p21* transcripts decayed slowly in MKN28 cells, and the depletion of PARN did not affect the decay rate. A rapid decay of the *p21* transcripts was observed in AGS cells with a half-life of ~1 h. PARN-knockdown in AGS cells could successfully stabilize *p21* and the amounts of *p21* mRNAs remained unchanged within 4 h of actinomycin D treatment. Unlike in MKN28 cells, the expression levels of the other major mammalian deadenylases (Ccr4a, Ccr4b, Ccr4d, Caf1a, Caf1b and PAN2–PAN3) were unaffected by knockdown of PARN in AGS cells (Fig. 8C and D, right panels). Thus it seems that the stabilization of *p21* mRNAs was directly linked to PARN-depletion in AGS cells.

Luciferase assays were performed for the promoter and UTR of *p21* to further investigate whether PARN triggered the decay of the *p21* transcripts directly or not. The PARN-depleted MKN28 and AGS cells were transfected with the *p21* promoter-, 5′-UTR- or 3′-UTR-driven luciferase reporter constructs as described previously [21]. The luciferase activities of the cell lysates were determined after 24 h transfection and the results are shown in Fig. 8E. Consistent with the mRNA stability results, the luciferase activities were almost identical for all those assayed in MKN28 cells. As for AGS cells, no significant difference was observed between the control and PARN-depleted cells when transfected with the *p21* promoter- or 5′-UTR-driven luciferase reporter constructs. A three-fold increase in the luciferase activity was induced by PARN-depletion when the luciferase gene expressed in AGS cells was driven by *p21* 3′-UTR. Thus the results in Fig. 8 suggested that the *p21* mRNA was degraded in a deadenylation-dependent pathway directly mediated by PARN in AGS cells but not in MKN28 cells. The accumulation of steady-state *p21* in the PARN-depleted MKN28 cells was more likely to be an indirect effect of PARN-knockdown, probably by the compensatory expression of Ccr4d (left panel of Fig. 8C).

4. Discussion

Although the mechanism of deadenylase function remains a huge challenge, it is increasingly clear that various deadenylases play an important role in diverse cellular processes by regulating mRNA fates. Particularly, some members in both of the Ccr4 and Caf1 families have been found to participate in cell proliferation. Depletion of Ccr4b/CNOT6L retards the growth of NIH 3T3 cells by increasing the mRNA stability of *p27* [26]. Overexpression of Ccr4d/ANGEL2 inhibits the proliferation of MCF-7 cells by elevating *p21* mRNA stability [21]. Caf1a/CNOT7 and Caf1b/CNOT8 has been identified to be anti-proliferation proteins through binding with B-cell translocation gene proteins (BTG1 and BTG2) [42–47]. Ccr4a/CNOT6 and Ccr4b/CNOT6L contribute to cell survival and the prevention of cell death and senescence [48]. In this research, we showed that depletion of PARN significantly retarded the proliferation of two types of gastric cancer cells via stabilizing the mRNA stability of *p21*. To our knowledge, this is the first deadenylase that is identified to effectively destabilize the *p21* mRNA, one of the key regulators in cell growth and survival.

PARN is highly conserved in higher eukaryotes, but is not identified in yeast and fly [2,4,5]. Previous functional studies have shown that

PARN is involved in several crucial physiological processes such as the meiotic maturation of frog oocytes [49], embryogenesis and stress response in plants [50,51] and stage-specific protein production in *Trypanosoma brucei* [52]. As for the cellular processes, PARN can regulate cell motility in mouse myoblasts [33], maturation of mammalian H/ACA box snoRNA [53], miRNA biogenesis [54] and DNA damage response (DDR) [31,32,55]. Although the intact picture of PARN functions has not been fully deciphered yet, the above pioneering studies have strongly support the opinion that PARN is not a major deadenylase for cytoplasmic deadenylation, but mainly functions in highly regulated mRNA decay by targeting a small subset of mRNAs [5,33]. Our results also support such an opinion since the depletion of PARN did not affect the formation of nuclear and cytoplasmic poly(A)$^+$ foci including P-bodies (Fig. 7). Meanwhile, among the cell proliferation regulators tested here, PARN-depletion only affects the decay rate of *p21* mRNA.

Although it is clear that PARN participates into a certain cellular process by specifically modulating the stability of a small subset of mRNAs [33], the action of PARN seems to strongly depend on the status or protein expression profiles of the cells. Previously PARN-knockdown has been shown to reduce cell adhesion and cell movement of mouse C2Cl2 myoblasts [33]. However, our results suggested that PARN was not required for the migration and invasion of two different gastric cancer cell lines, MKN28 and AGS. More importantly, although growth inhibition induced by PARN-depletion was observed for both of MKN28 and AGS cells, the underlying mechanisms might be quite different. Both cells had elevated expression levels of p53 and p21. Previously it has been shown that *p53* is one of the targets of PARN in the HCT116 cells under nonstressed conditions [55]. However, herein we showed that the stability of the *p53* mRNA was unaffected by PARN amounts in gastric cancer cells. PARN-depletion might affect factors regulating p53, but not target *p53* directly. The depletion of PARN significantly increased *p21* mRNA stability in AGS cells but not in MKN28 cells. Thus PARN targeted the *p21* mRNA 3′-UTR and trigged its decay directly in the AGS cells, but affected the *p21* mRNA stability via an indirect and complicated pathway in the MKN28 cells. One of the major differences between the MKN28 and AGS cells is that AGS possesses wild-type p53, while MKN28 has a mutated one [56]. Thus it seemed that the increased amount of p53 did not contribute to the upregulation of p21 in MKN28 cells. A possible reason is the compensatory expression increase of Ccr4d/ANGEL2, which has been shown to stabilize *p21* in MCF-7 cells by elevating *p21* mRNA stability [21]. It is unclear yet why a compensatory effect of deadenylase expression was induced in MKN28 but not AGS cells by PARN-knockdown. Nonetheless, the dissimilar effect of PARN-depletion on *p21* stability in the two types of gastric cells suggested that the action of PARN may be precisely regulated though PARN has the intrinsic property to trigger *p21* decay.

The strong dependence of PARN function on cellular conditions was also observed in the action of PARN during DDR. The 80 kDa subunit of the cap-binding complex (CBP80) can inhibit the deadenylase activity of PARN [57]. During DDR, the cleavage stimulation factor-50 (CstF-50) removes the inhibition effect of CBP80 and activates PARN in the HeLa cells. Lately p38/MK2 has been shown to be able to phosphorylate PARN during DDR, which subsequently releases the *Gadd45α* mRNAs from the degradation pathway in the p53-defective tumor cells [55]. Very recently PARN has been proposed to be activated by the binding of p53 during DDR in the colon cancer HCT116 cells [55]. A close inspection into the results in literature as well as the results herein strongly support the opinion that the cellular functions of deadenylase are dependent on the protein expression profile of a certain type of cells or under a given stress condition. Our results also suggested that besides the well-characterized genetic heterogeneity in cancers, the heterogeneity at the post-transcriptional level such as mRNA stability could not be neglected in mechanistic studies and drug design.

It remains unclear for the *cis*-acting element(s) and *trans*-acting factor(s) mediating the targeting of PARN to the *p21* mRNA 3′-UTR. We failed to pull-down potential PARN binding partners by immunoprecipitation experiments. Although a significant difference was observed between the two types of gastric cancer cells, the same phenotype but different mechanisms also raise a big challenge to identify the key regulators mediating the action of PARN. Nonetheless, it is clear that the 3′-UTR but not the promoter in the DNA, ORF or 5′-UTR in the *p21* mRNA is the key region containing PARN-responsive *cis*-acting element(s). As mentioned in Section 1, the *p21* mRNA possesses a long 3′-UTR and several *cis*-acting elements such as ARE has been identified. However, most elements and the corresponding factors have been found to stabilize *p21* [15]. Recently, several *p21*-destabilizing RNA-binding proteins have been identified in certain cell types [22–24]. However, it remains elusive for the relationship between these RNA-binding proteins and the various deadenylases.

Accumulating evidence supports the idea that mRNA decay plays a crucial role in human health and diseases. However, the knowledge remains very limited for the regulators of mRNA decay and the pairwise relationships for elements–factors–deadenylases [2]. PARN has been proposed to be a potential target of cancer treatment [7] and is highly expressed in acute leukemias [34] and gastric cancers (this research). Further research is needed to fully decipher the physiological/pathological functions and the key mRNA targets of PARN as well as the other deadenylases.

Acknowledgements

We thank Prof. Shang YF and Dr. Yi X (Peking University) for kindly providing the *p21* promoter and 3′-UTR firefly luciferase constructs, Prof. Zhou HM and Dr. Li J (Tsinghua University) for kindly providing the cDNAs of gastric cancer tissue samples, Dr. Li J (Tsinghua University) for suggestions in cell proliferation and migration assays, Dr. Li J, Dr. Chen Z and Dr. Mo ML (Tsinghua University) for suggestions in the establishment of PARN-depletion stable cell lines, Mr. Yu Q for help with plasmid construction, Prof. Wu W (Tsinghua University) for help with the luciferase activity assay and the Cell Core Facility at Tsinghua University for carrying out the microscopy and FACS studies. This work was funded by National Natural Science Foundation of China (31370797).

Appendix A. Supplementary data

The supplemental material contains ten supporting figures. Supplementary data associated with this article can be found, in the online version, at http://dx.doi.org/10.1016/j.bbamcr.2014.12.004.

References

[1] G. Caponigro, R. Parker, Mechanisms and control of mRNA turnover in *Saccharomyces cerevisiae*, Microbiol. Rev. 60 (1996) 233–249.
[2] Y.B. Yan, Deadenylation: enzymes, regulation, and functional implications, Wiley Interdiscip. Rev. RNA 5 (2014) 421–443.
[3] N.L. Garneau, J. Wilusz, C.J. Wilusz, The highways and byways of mRNA decay, Nat. Rev. Mol. Cell Biol. 8 (2007) 113–126.
[4] A.C. Goldstrohm, M. Wickens, Multifunctional deadenylase complexes diversify mRNA control, Nat. Rev. Mol. Cell Biol. 9 (2008) 337–344.
[5] A. Virtanen, N. Henriksson, P. Nilsson, M. Nissbeck, Poly(A)-specific ribonuclease (PARN): an allosterically regulated, processive and mRNA cap-interacting deadenylase, Crit. Rev. Biochem. Mol. Biol. 48 (2013) 192–209.
[6] A.R. Godwin, S. Kojima, C.B. Green, J. Wilusz, Kiss your tail goodbye: the role of PARN, Nocturnin, and Angel deadenylases in mRNA biology, Biochim. Biophys. Acta 1829 (2013) 571–579.
[7] N.A. Balatsos, P. Maragozidis, D. Anastasakis, C. Stathopoulos, Modulation of poly(A)-specific ribonuclease (PARN): current knowledge and perspectives, Curr. Med. Chem. 19 (2012) 4838–4849.
[8] S.L. Moon, J. Wilusz, Cytoplasmic viruses: rage against the (cellular RNA decay) machine, PLoS Pathog. 9 (2013) e1003762.
[9] I. Groisman, M.Y. Jung, M. Sarkissian, Q. Cao, J.D. Richter, Translational control of the embryonic cell cycle, Cell 109 (2002) 473–483.
[10] C.J. Sherr, J.M. Roberts, CDK inhibitors: positive and negative regulators of G1-phase progression, Genes Dev. 13 (1999) 1501–1512.
[11] A. Besson, S.F. Dowdy, J.M. Roberts, CDK inhibitors: cell cycle regulators and beyond, Dev. Cell 14 (2008) 159–169.

[12] T. Riley, E. Sontag, P. Chen, A. Levine, Transcriptional control of human p53-regulated genes, Nat. Rev. Mol. Cell Biol. 9 (2008) 402–412.
[13] O. Coqueret, New roles for p21 and p27 cell-cycle inhibitors: a function for each cell compartment? Trends Cell Biol. 13 (2003) 65–70.
[14] N.A. Warfel, W.S. El-Deiry, p21WAF1 and tumourigenesis: 20 years after, Curr. Opin. Oncol. 25 (2013) 52–58.
[15] Y.S. Jung, Y. Qian, X. Chen, Examination of the expanding pathways for the regulation of p21 expression and activity, Cell. Signal. 22 (2010) 1003–1012.
[16] B. Joseph, M. Orlian, H. Furneaux, p21(waf1) mRNA contains a conserved element in its 3′-untranslated region that is bound by the Elav-like mRNA-stabilizing proteins, J. Biol. Chem. 273 (1998) 20511–20516.
[17] S.S. Peng, C.Y. Chen, N. Xu, A.B. Shyu, RNA stabilization by the AU-rich element binding protein, HuR, an ELAV protein, EMBO J. 17 (1998) 3461–3470.
[18] Y. Jiang, M. Zhang, Y. Qian, E. Xu, J. Zhang, X. Chen, Rbm24, an RNA-binding protein and a target of p53, regulates p21 expression via mRNA stability, J. Biol. Chem. 289 (2014) 3164–3175.
[19] L. Shu, W. Yan, X. Chen, RNPC1, an RNA-binding protein and a target of the p53 family, is required for maintaining the stability of the basal and stress-induced p21 transcript, Genes Dev. 20 (2006) 2961–2972.
[20] M. Nie, M.S. Balda, K. Matter, Stress- and Rho-activated ZO-1-associated nucleic acid binding protein binding to p21 mRNA mediates stabilization, translation, and cell survival, Proc. Natl. Acad. Sci. U. S. A. 109 (2012) 10897–10902.
[21] X. Yi, M. Hong, B. Gui, Z. Chen, L. Li, G. Xie, J. Liang, X. Wang, Y. Shang, RNA processing and modification protein, carbon catabolite repression 4 (Ccr4), arrests the cell cycle through p21-dependent and p53-independent pathway, J. Biol. Chem. 287 (2012) 21045–21057.
[22] A. Scoumanne, S.J. Cho, J. Zhang, X. Chen, The cyclin-dependent kinase inhibitor p21 is regulated by RNA-binding protein PCBP4 via mRNA stability, Nucleic Acids Res. 39 (2011) 213–224.
[23] S.A. Waggoner, G.J. Johannes, S.A. Liebhaber, Depletion of the poly(C)-binding proteins αCP1 and αCP2 from K562 cells leads to p53-independent induction of cyclin-dependent kinase inhibitor (CDKN1A) and G1 arrest, J. Biol. Chem. 284 (2009) 9039–9049.
[24] L. Davidovic, N. Durand, O. Khalfallah, R. Tabet, P. Barbry, B. Mari, S. Sacconi, H. Moine, B. Bardoni, A novel role for the RNA-binding protein FXR1P in myoblasts cell-cycle progression by modulating p21/Cdkn1a/Cip1/Waf1 mRNA stability, PLoS Genet. 9 (2013) e1003367.
[25] C.Y. Chen, A.B. Shyu, Mechanisms of deadenylation-dependent decay, Wiley Interdiscip. Rev. RNA 2 (2011) 167–183.
[26] M. Morita, T. Suzuki, T. Nakamura, K. Yokoyama, T. Miyasaka, T. Yamamoto, Depletion of mammalian CCR4b deadenylase triggers elevation of the p27Kip1 mRNA level and impairs cell growth, Mol. Cell. Biol. 27 (2007) 4980–4990.
[27] W.-J. Lin, A. Duffy, C.-Y. Chen, Localization of AU-rich element-containing mRNA in cytoplasmic granules containing exosome subunits, J. Biol. Chem. 282 (2007) 19958–19968.
[28] R. Gherzi, K.Y. Lee, P. Briata, D. Wegmuller, C. Moroni, M. Karin, C.Y. Chen, A KH domain RNA binding protein, KSRP, promotes ARE-directed mRNA turnover by recruiting the degradation machinery, Mol. Cell 14 (2004) 571–583.
[29] W.S. Lai, E.A. Kennington, P.J. Blackshear, Tristetraprolin and its family members can promote the cell-free deadenylation of AU-rich element-containing mRNAs by poly(A) ribonuclease, Mol. Cell. Biol. 23 (2003) 3798–3812.
[30] K.C.M. Moraes, C.J. Wilusz, J. Wilusz, CUG-BP binds to RNA substrates and recruits PARN deadenylase, RNA 12 (2006) 1084–1091.
[31] H.C. Reinhardt, P. Hasskamp, I. Schmedding, S. Morandell, M.A. van Vugt, X. Wang, R. Linding, S.E. Ong, D. Weaver, S.A. Carr, M.B. Yaffe, DNA damage activates a spatially distinct late cytoplasmic cell-cycle checkpoint network controlled by MK2-mediated RNA stabilization, Mol. Cell 40 (2010) 34–49.
[32] M.A. Cevher, X. Zhang, S. Fernandez, S. Kim, J. Baquero, P. Nilsson, S. Lee, A. Virtanen, F.E. Kleiman, Nuclear deadenylation/polyadenylation factors regulate 3′ processing in response to DNA damage, EMBO J. 29 (2010) 1674–1687.
[33] J.E. Lee, J.Y. Lee, J. Trembly, J. Wilusz, B. Tian, C.J. Wilusz, The PARN deadenylase targets a discrete set of mRNAs for decay and regulates cell motility in mouse myoblasts, PLoS Genet. 8 (2012) e1002901.
[34] P. Maragozidis, M. Karangeli, M. Labrou, G. Dimoulou, K. Papaspyrou, E. Salataj, S. Pournaras, P. Matsouka, K.I. Gourgoulianis, N.A. Balatsos, Alterations of deadenylase expression in acute leukemias: evidence for poly(a)-specific ribonuclease as a potential biomarker, Acta Haematol. 128 (2012) 39–46.
[35] J. Li, M. Mo, Z. Chen, Z. Chen, Q. Sheng, H. Mu, F. Zhang, Y. Zhang, X.Y. Zhi, H. Li, B. He, H.M. Zhou, Adenoviral delivery of the EMX2 gene suppresses growth in human gastric cancer, PLoS One 7 (2012) e45970.
[36] M. Bühler, M.F. Wilkinson, O. Mühlemann, Intranuclear degradation of nonsense codon-containing mRNA, EMBO Rep. 3 (2002) 646–651.
[37] D.R. Rhodes, S. Kalyana-Sundaram, V. Mahavisno, R. Varambally, J. Yu, B.B. Briggs, T.R. Barrette, M.J. Anstet, C. Kincead-Beal, P. Kulkarni, S. Varambally, D. Ghosh, A.M. Chinnaiyan, Oncomine 3.0: genes, pathways, and networks in a collection of 18,000 cancer gene expression profiles, Neoplasia 9 (2007) 166–180.
[38] K. Kozar, M.A. Ciemerych, V.I. Rebel, H. Shigematsu, A. Zagozdon, E. Sicinska, Y. Geng, Q.Y. Yu, S. Bhattacharya, R.T. Bronson, K. Akashi, P. Sicinski, Mouse development and cell proliferation in the absence of D-cyclins, Cell 118 (2004) 477–491.
[39] M. van Engeland, L.J.W. Nieland, F.C.S. Ramaekers, B. Schutte, C.P.M. Reutelingsperger, Annexin V-affinity assay: a review on an apoptosis detection system based on phosphatidylserine exposure, Cytometry 31 (1998) 1–9.
[40] D.L. Spector, SnapShot: cellular bodies, Cell 127 (2006) 1071.
[41] N. Cougot, S. Babajko, B. Seraphin, Cytoplasmic foci are sites of mRNA decay in human cells, J. Cell Biol. 165 (2004) 31–40.
[42] J.A. Bogdan, C. Adams-Burton, D.L. Pedicord, D.A. Sukovich, P.A. Benfield, M.H. Corjay, J.K. Stoltenborg, I.B. Dicker, Human carbon catabolite repressor protein (CCR4)-associative factor 1: cloning, expression and characterization of its interaction with the B-cell translocation protein BTG1, Biochem. J. 336 (1998) 471–481.
[43] D. Prevot, A.-P. Morel, T. Voeltzel, M.-C. Rostan, R. Rimokh, J.-P. Magaud, L. Corbo, Relationships of the antiproliferative proteins BTG1 and BTG2 with CAF1, the human homolog of a component of the yeast CCR4 transcriptional complex: involvement in estrogen receptor alpha signaling pathway, J. Biol. Chem. 276 (2001) 9640–9648.
[44] A. Aslam, S. Mittal, F. Koch, J.C. Andrau, G.S. Winkler, The Ccr4-NOT deadenylase subunits CNOT7 and CNOT8 have overlapping roles and modulate cell proliferation, Mol. Biol. Cell 20 (2009) 3840–3850.
[45] R. Doidge, S. Mittal, A. Aslam, G.S. Winkler, The anti-proliferative activity of BTG/TOB proteins is mediated via the Caf1a (CNOT7) and Caf1b (CNOT8) deadenylase subunits of the Ccr4-not complex, PLoS One 7 (2012) e51331.
[46] A.P. Morel, S. Sentis, C. Bianchin, M. Le Romancer, L. Jonard, M.C. Rostan, R. Rimokh, L. Corbo, BTG2 antiproliferative protein interacts with the human CCR4 complex existing in vivo in three cell-cycle-regulated forms, J. Cell Sci. 116 (2003) 2929–2936.
[47] N. Hosoda, Y. Funakoshi, M. Hirasawa, R. Yamagishi, Y. Asano, R. Miyagawa, K. Ogami, M. Tsujimoto, S. Hoshino, Anti-proliferative protein Tob negatively regulates CPEB3 target by recruiting Caf1 deadenylase, EMBO J. 30 (2011) 1311–1323.
[48] S. Mittal, A. Aslam, R. Doidge, R. Medica, G.S. Winkler, The Ccr4a (CNOT6) and Ccr4b (CNOT6L) deadenylase subunits of the human Ccr4-Not complex contribute to the prevention of cell death and senescence, Mol. Biol. Cell 22 (2011) 748–758.
[49] C.G. Korner, M. Wormington, M. Muckenthaler, S. Schneider, E. Dehlin, E. Wahle, The deadenylating nuclease (DAN) is involved in poly(A) tail removal during the meiotic maturation of Xenopus oocytes, EMBO J. 17 (1998) 5427–5437.
[50] S.V. Reverdatto, J.A. Dutko, J.A. Chekanova, D.A. Hamilton, D.A. Belostotsky, MRNA deadenylation by PARN is essential for embryogenesis in higher plants, RNA 10 (2004) 1200–1214.
[51] N. Nishimura, N. Kitahata, M. Seki, Y. Narusaka, M. Narusaka, T. Kuromori, T. Asami, K. Shinozaki, T. Hirayama, Analysis of ABA *Hypersensitive Germination2* revealed the pivotal functions of PARN in stress response in Arabidopsis, Plant J. 44 (2005) 972–984.
[52] C.J. Utter, S.A. Garcia, J. Milone, V. Bellofatto, PolyA-specific ribonuclease (PARN-1) function in stage-specific mRNA turnover in *Trypanosoma brucei*, Eukaryot. Cell 10 (2011) 1230–1240.
[53] H. Berndt, C. Harnisch, C. Rammelt, N. Stohr, A. Zirkel, J.C. Dohm, H. Himmelbauer, J.P. Tavanez, S. Huttelmaier, E. Wahle, Maturation of mammalian H/ACA box snoRNAs: PAPD5-dependent adenylation and PARN-dependent trimming, RNA 18 (2012) 958–972.
[54] M. Yoda, D. Cifuentes, N. Izumi, Y. Sakaguchi, T. Suzuki, A.J. Giraldez, Y. Tomari, Poly(A)-specific ribonuclease mediates 3′-end trimming of Argonaute2-cleaved precursor microRNAs, Cell Rep. 5 (2013) 715–726.
[55] E. Devany, X. Zhang, J.Y. Park, B. Tian, F.E. Kleiman, Positive and negative feedback loops in the p53 and mRNA 3′ processing pathways, Proc. Natl. Acad. Sci. U. S. A. 110 (2013) 3351–3356.
[56] H. Yokozaki, Molecular characteristics of eight gastric cancer cell lines established in Japan, Pathol. Int. 50 (2000) 767–777.
[57] N.A. Balatsos, P. Nilsson, C. Mazza, S. Cusack, A. Virtanen, Inhibition of mRNA deadenylation by the nuclear cap binding complex (CBC), J. Biol. Chem. 281 (2006) 4517–4522.